

Estimated strength of the Atlantic overturning circulation during the last deglaciation

Author:

Ritz, S; Stocker, T; Grimalt, J; Menviel, Laurie; Timmermann, A

Publication details:

Nature Geoscience

v. 6

Chapter No. 3

pp. 208-212

1752-0894 (ISSN)

Publication Date:

2013

Publisher DOI:

<http://dx.doi.org/10.1038/ngeo1723>

License:

<https://creativecommons.org/licenses/by-nc-nd/3.0/au/>

Link to license to see what you are allowed to do with this resource.

Downloaded from <http://hdl.handle.net/1959.4/53719> in <https://unsworks.unsw.edu.au> on 2024-04-20

Estimated strength of Atlantic overturning circulation during the last deglaciation

STEFAN P. RITZ, * THOMAS F. STOCKER

Climate and Environmental Physics, Physics Institute, University of Bern, Bern, Switzerland

and Oeschger Centre for Climate Change Research, University of Bern, Bern, Switzerland

JOAN O. GRIMALT

Department of Environmental Chemistry, Institute of Environmental Assessment and Water Research,

Spanish Council for Scientific Research, Barcelona, Spain

LAURIE MENVIEL

Climate Change Research Centre, Centre of Excellence, University of New South Wales, Sydney, Australia

AXEL TIMMERMANN

IPRC, University of Hawaii, Honolulu, USA

* *Corresponding author address:* Stefan P. Ritz, University of Bern, Physics Institute, Climate and Environmental Physics, Sidlerstr. 5, 3012 Bern, Switzerland
E-mail: ritz@climate.unibe.ch

1 The reconstruction of the state and strength of the Atlantic meridional overturning circu-
 2 lation (AMOC) in the past is an important topic in paleoceanography. Many proxies have
 3 been proposed that give information on the state of the past circulation¹. Of these, only the
 4 protactinium-to-thorium ($^{231}\text{Pa}/^{230}\text{Th}$) activity ratio of ocean sediments and top-to-bottom ra-
 5 diocarbon age differences provide qualitative estimates of changes in the AMOC strength^{2,3,4,5}.
 6 But the robustness of these indicators is still under debate^{6,7,8}. Here we reconstruct changes
 7 in the AMOC strength over the period of the last deglaciation quantitatively by using a novel
 8 method, which derives changes in the ocean circulation from a combination of time series re-
 9 constructions of sea surface temperature (SST) and air temperature. A global climate model
 10 provides the relationship between SST, air temperature, and AMOC strength. Our recon-
 11 struction of the changes in the AMOC strength during the last deglaciation is consistent with
 12 qualitative reconstructions from sedimentary $^{231}\text{Pa}/^{230}\text{Th}$. It suggests an AMOC reduction
 13 of about 14 Sv (Sverdrup; $1\text{ Sv} = 10^6\text{ m}^3\text{ s}^{-1}$) during Heinrich stadial 1 compared to the Last
 14 Glacial Maximum (LGM), and a slightly lower reduction during the Younger Dryas cold event.
 15 The difference between the AMOC strength during the LGM and the Holocene lies within
 16 the uncertainty of the reconstruction.

17 The AMOC is an important feature of the Earth's climate system. It is characterized by northward flowing
 18 water masses at the surface ocean, deep water formation in the North Atlantic and southward flowing water
 19 masses in the intermediate to deep ocean. This overturning cell is complemented by an underlying, generally
 20 weaker, reversed overturning cell that originates in the Southern Ocean. In the following, we use AMOC
 21 to refer only to the upper overturning cell. Because of the large heat capacity of water, the northward
 22 flowing near-surface waters contribute effectively to the heat transport from the tropics to the mid- and
 23 high latitudes and therefore affect the regional climate around the North Atlantic^{9,10}. Hence, changes of
 24 the AMOC strength can substantially influence climate in the north, especially in Europe. The depth of
 25 the southward flowing waters as well as the strength of the circulation have changed in the past. During
 26 the last glacial period, abrupt warming events of several degrees within a few decades followed by slower
 27 cooling were detected in Greenland ice cores¹¹. Because effects of the so-called Dansgaard-Oeschger events

were found far beyond the Greenland ice sheet^{12,13,14} with patterns reminiscent of varying inter-hemispheric heat distribution^{15,16}, they are believed to be the result of rapid changes of the AMOC strength¹⁷. Other examples of a reduction or even a complete shutdown of the AMOC are Heinrich stadial 1 from approximately 16.8 to 14.6 ka before present (B.P., before year 1950 AD)¹⁸, the Younger Dryas stadial from approximately 12.8 to 11.6 ka B.P.¹⁹ and the 8.2 ka event²⁰.

In this study, we present a numerical reconstruction scheme to infer the past evolution of the AMOC strength on centennial to glacial-interglacial timescales. The scheme is based on earlier work²¹ that proposes that ocean temperature anomalies at any location (i), T_{oc}^i , can be approximated by a linear combination of anomalies of global mean air temperature (T'_{atm}), AMOC (Ψ'_{AMOC}), and Southern Ocean meridional overturning circulation (SOMOC) strength. The strength of the circulation is defined by the maximum of the meridional overturning stream function. In this study we focus on the surface Atlantic, where the effect of the SOMOC can be neglected²¹. Hence, we can linearly approximate the time evolution of the surface temperature pattern $T_{oc}^i(t)$ as

$$T_{oc}^i(t) = a_{Tatm}^i \cdot T'_{atm}(t) + a_{AMOC}^i \cdot \Psi'_{AMOC}(t). \quad (1)$$

The relationships between Atlantic SST, air temperature and AMOC are the result of ocean dynamics, and we determine coefficients (a_{Tatm}^i and a_{AMOC}^i) describing the postulated linear relationships using a global climate model, subject to a combination of forcings (see Methods section). Global mean air temperature time series can be determined from air temperature reconstructions from Antarctic ice cores²² and SST time series reconstructions are available from several marine sediment cores. Hence, Eq. (1) can be solved for Ψ'_{AMOC} . When several SST records are incorporated into the reconstruction, a least squares solution can be calculated:

$$\Psi'_{AMOC}(t) = \sum_{i=1}^n \frac{w_i}{a_{AMOC}^i} [T_{oc}^i(t) - a_{Tatm}^i T'_{atm}(t)], \quad (2)$$

where w_i is the weight of location i and is determined by the least squares solver.

The simplicity of our assumption requires thorough testing of the reconstruction method. This is accomplished by hindcasting the AMOC strength of two model simulations from two independent climate models.

Also, the coefficients of the reconstruction scheme are calculated by two independent models (Fig. 1): By an ensemble of simulations performed with the Bern3D Earth System Model of intermediate complexity (shorthand B3D; Supplementary information; Fig. S2; Table S3), and by a transient deglaciation simulation performed using the LOVECLIM Earth System Model of intermediate complexity²³ (shorthand LVC; Supplementary information; Fig. S4; Table S4). In both cases a broad range of climate states is generated in response to various freshwater and CO₂ forcings that alter the AMOC, SST and global mean air temperature, respectively. Using the coefficients derived from the B3D and the LVC sensitivity experiments, AMOC hindcasts are calculated for the LVC simulation, and for a freshwater forcing simulation conducted with the NCAR CSM1.4 coupled atmosphere-ocean general circulation model²⁴ (shorthand CSM; Supplementary information; Fig. S5).

For the AMOC hindcasts, we substitute the real world by one of the model simulations and “reconstruct” the AMOC evolution based on our method using simulated SST time series from several Atlantic locations as well as global mean air temperature time series. The reconstructed AMOC evolution can then be compared to the temporal evolution of the true model AMOC. For both AMOC hindcasts, 14 model SST time series of the Atlantic Ocean are used (Fig. S1). The locations of the time series correspond to locations where real SST reconstructions of the last deglaciation are available with an average resolution of at least 500 years (Table S1). These SST records will be used later for the reconstruction of the deglacial AMOC variability.

As a first test, an AMOC hindcast of the LVC simulation is calculated, where the reconstruction scheme coefficients are also determined from the LVC simulation (Fig. 2a). The hindcast correlates well with the modeled AMOC ($R = 0.97$) and the relative standard deviation of $s_{\text{rel}} = 1.03$ is close to the optimum value of 1 (s_{rel} is defined as the standard deviation of the hindcasted AMOC divided by the standard deviation of the modeled AMOC). The LVC hindcast is also successful when coefficients determined from the B3D simulations are used ($R = 0.97$, $s_{\text{rel}} = 0.85$; Fig. 2a). The largest discrepancy between hindcast and model AMOC appears during the Bølling between 15 and 14 ka B.P., where the AMOC peak of the model is not captured by the hindcast. The peak would be somewhat better captured if SSTs from the central North Atlantic (at approximately 50°N, 35°W) were incorporated into the hindcast (Fig. S6). Unfortunately, there are currently no paleo-SST reconstructions available from this region and hence we have not included this

region in our analysis.

The weights that the least squares solver assigns to the individual SST locations determines the relative contributions of the individual SST time series to the AMOC hindcast. The smaller the weight, the less sensitive the temperature at the particular location is to changes of AMOC strength. The six northeastern Atlantic SST time series together have the largest influence on the hindcasts and account for a cumulative weight of ca. 90 % (see Table S5 for a list of the weights).

Next, the AMOC of the CSM model is hindcasted (Fig. 2b). The atmospheric component of this model is considerably more complex than LVC. Again, both hindcasts calculated using LVC and B3D coefficients are very similar and compare well with the CSM model AMOC (for LVC coefficients: $R = 0.98$, $s_{\text{rel}} = 1.12$; for B3D coefficients: $R = 0.97$, $s_{\text{rel}} = 0.96$).

The hindcasts of the LVC deglaciation simulation and of the CSM freshwater forcing simulation emphasize the robustness of the AMOC reconstruction method. In the following, we apply the method to Atlantic SST reconstructions from marine sediment cores to estimate the AMOC anomalies of the last deglaciation. One of the 14 SST records only goes back to 19 ka B.P. We do not use this record for the AMOC reconstruction in order to extend the reconstruction back to the LGM. Because of the small weight of this location, this has little impact on the result. The SST data are splined using a cutoff period of $\tau_{\text{cut}} = 1000$ years. Since there is no direct proxy for global mean air temperature, it is determined from the Antarctic air temperature reconstruction from the EPICA Dome C ice core²⁵ by lowpass filtering the data using a cutoff period of 10 ka to remove local-to-hemispheric scale variability (such as the Antarctic Cold Reversal) and by applying a polar amplification factor of 2 which is determined from comprehensive global atmosphere-ocean general circulation models from the Paleoclimate Modelling Intercomparison Projects PMIP-1 and PMIP-2²².

Two AMOC reconstructions are presented: one using coefficients calculated from the B3D simulation, and one using coefficients calculated from the LVC simulation (Fig. 3). The 1σ -uncertainty band of the AMOC reconstruction follows from Gaussian uncertainty propagation of the individual uncertainties (Supplementary information). These are the uncertainties of the SST reconstructions (Table S1) and the air temperature reconstruction ($\pm 1.5^\circ\text{C}$), the uncertainties of the age scales of the individual temperature reconstructions

(± 500 yr for the last deglaciation), and the uncertainties of the coefficients of the reconstruction scheme. The uncertainty band is calculated separately for the reconstruction using the B3D coefficients and for the reconstruction using the LVC coefficients.

The two reconstructions are very similar (Fig. 3). The AMOC during Heinrich stadial 1 (H1) appears to be approximately 14 Sv weaker than during the LGM with a range of 5 to 23 Sv decrease. With a present-day AMOC strength of around $19 \text{ Sv} \pm 5 \text{ Sv}^{26}$, this suggests a substantial slowdown of the AMOC during H1. The reconstruction also shows an AMOC slowdown during the Younger Dryas (YD) by 12 Sv with a range of 5 to 22 Sv decrease in circulation compared to the Bølling/Allerød. The reconstruction is consistent with the AMOC reconstruction by McManus et al². However, our reconstruction suggests a stronger reduction of the AMOC during the YD. Furthermore, the LGM-to-Holocene AMOC difference is less prominent in our reconstruction than in the $^{231}\text{Pa}/^{230}\text{Th}$ data.

We can use our method to inform about locations for SST records which would be most effective for an AMOC reconstruction. Eq. (2) can be rearranged to

$$\Psi'_{\text{AMOC}}(t) = \sum_{i=1}^n \frac{w_i}{a_{\text{AMOC}}^i} T_{\text{oc}}^i(t) - \beta T'_{\text{atm}}(t), \quad (3)$$

where $\beta = \sum_{i=1}^n (w_i a_{\text{Tatm}}^i / a_{\text{AMOC}}^i)$, and w_i / a_{AMOC}^i is the spatial fingerprint of the AMOC. It determines the influence of every location (i) on the AMOC hindcast. To assess these fingerprints, we calculated an AMOC hindcast of the CSM simulation based on SST time series of every LVC surface Atlantic model cell and by using reconstruction scheme coefficients determined from the LVC model (Fig. 4). Not surprisingly, the result is a bipolar seesaw pattern with largest fingerprints in the North East Atlantic.

Our AMOC reconstruction method can also be applied on longer timescales to reconstruct the AMOC over multiple glacial-interglacial cycles. However, a substantially larger age-scale uncertainty must be applied when radiocarbon dating is not available. Furthermore, changes of other large scale circulations can potentially be reconstructed such as the Southern Ocean meridional overturning circulation (SOMOC). In this case, deep ocean temperature time series reconstructions would be suitable candidates for the reconstruction. If deep ocean temperature reconstructions are included, then time lags between changes in air

temperature, ocean circulation, and ocean temperatures need to be allowed for in Eq. (1), i.e. $T'_{\text{atm}}(t - \tau_{\text{Tatm}}^i)$ and $\Psi'_{\text{SOMOC}}(t - \tau_{\text{SOMOC}}^i)$. Further, a possible occurrence of a North Pacific meridional overturning circulation (NPMOC) cell during Heinrich stadials could be reconstructed²⁷. However, both SOMOC and NPMOC reconstructions would require further ocean temperature time series reconstructions at locations that are sensitive to these circulation changes.

Methods

Methodology

The reconstruction of the AMOC strength is based on the assumption that on centennial to glacial-interglacial timescales, SST anomalies (T_{oc}^i) at any location in the Atlantic i can be approximated by a linear combination of global mean air temperature anomalies (T'_{atm}) and AMOC strength anomalies (Ψ'_{AMOC}):

$$T_{\text{oc}}^i(t) = a_{\text{Tatm}}^i \cdot T'_{\text{atm}}(t) + a_{\text{AMOC}}^i \cdot \Psi'_{\text{AMOC}}(t).$$

We define the AMOC strength as the maximum of the Atlantic meridional overturning stream function. Anomalies are defined as $T_{\text{oc}}^i(t) = T_{\text{oc}}^i(t) - \bar{T}_{\text{oc}}^i$ with $T_{\text{oc}}^i(t)$ the SST at time t and \bar{T}_{oc}^i the temperature averaged over a period of time, and analogously for T'_{atm} and Ψ'_{AMOC} .

This approximation is supported by a recent study²⁸ in which a principal component analysis of globally distributed paleo-records of temperature revealed that 61 % of the climate variability of the last deglaciation can be explained by a globally near-uniform pattern that is strongly correlated to the atmospheric CO₂ change (representing global mean T'_{atm}), and 11 % can be explained by the bipolar seesaw pattern between the hemispheres¹⁶ which resembles the millennial-scale variability of the AMOC.

In this reconstruction scheme we also assume that coupled climate models are able to provide a reasonable physical relationship between changes of AMOC, air temperatures and ocean temperatures. Accepting these assumptions, then the coefficients of the reconstruction scheme, a_{Tatm}^i and a_{AMOC}^i , can be diagnosed from a

global coupled ocean-atmosphere climate model. Then with T'_{atm} time series reconstructions from ice cores and T'_{oc} time series reconstructions from marine sediment cores, Eq. (1) can be solved for Ψ'_{AMOC} .

A model simulation is performed where a broad range of climate states is produced by subjecting the model to various types of transient perturbations, e.g., by adding and removing freshwater from the North Atlantic to alter the AMOC strength, and e.g., by adding and removing CO_2 from the atmosphere to change air temperature. With this simulation we produce artificial climate reconstructions, i.e. purely model-based time series of $T'_{\text{oc}}, T'_{\text{atm}}$ and Ψ'_{AMOC} . At the location of every SST reconstruction (i), a^i_{Tatm} and a^i_{AMOC} are determined by multiple linear regression of the simulated SST evolution to the reconstruction scheme using the simulated global mean air temperature as well as the simulated AMOC strength:

$$(T'_{\text{oc}})^{\text{fit}}(t) = a^i_{\text{Tatm}} \cdot (T'_{\text{atm}})^{\text{model}}(t) + a^i_{\text{AMOC}} \cdot (\Psi'_{\text{AMOC}})^{\text{model}}(t), \quad (4)$$

and minimizing $J = \sum_{t_{\text{oc}}=t_{\text{st}}}^{t_{\text{end}}} [(T'_{\text{oc}})^{\text{fit}}(t_{\text{oc}}) - (T'_{\text{oc}})^{\text{model}}(t_{\text{oc}})]^2$. This results in estimates of the coefficients a^i_{Tatm} and a^i_{AMOC} (see Fig. S3 for examples). In this study, these coefficients are determined by an ensemble of 80 simulations performed with the B3D model, and by a deglaciation simulation using the LVC model²³ (Supplementary information).

T'_{atm} is ideally global mean air temperature, because AMOC changes hardly affect global mean temperatures. Global mean T'_{atm} captures temperature changes induced by changes of greenhouse gases and surface albedo. Unfortunately, to this date there is no direct paleoclimate proxy of global mean air temperature. It is therefore determined from an Antarctic air temperature reconstruction as described in the main text. Alternatively to global mean air temperatures, Antarctic air temperatures could be used, because T'_{atm} does not necessarily need to be independent of variations in AMOC (Fig. S7). It is important that in this case also Antarctic air temperatures are used for the determination of the coefficients of the reconstruction scheme. However, a prerequisite for this is that the polar amplification must be realistically represented in the model where the coefficients are determined. Furthermore, Antarctic air temperatures may additionally be influenced by quantities other than the AMOC which can lead to a systematic bias of the AMOC reconstruction.

173 Solving Eq. (1) for Ψ'_{AMOC} is trivial if only one SST time series reconstruction is used. If more than one T'_{oc}^i
 174 reconstruction is available, a least squares solution can be calculated:

$$\Psi'_{\text{AMOC}}(t) = \sum_{i=1}^n \frac{w_i}{a_{\text{AMOC}}^i} [T'_{\text{oc}}^i(t) - a_{\text{Tatm}}^i T'_{\text{atm}}(t)],$$

175 where w_i is the weight of location i and is determined by the least squares solver. Note that inaccurate
 176 coefficients a_{Tatm}^i may lead to a trend in Ψ'_{AMOC} in the case where T'_{oc}^i and T'_{atm} change simultaneously such
 177 as during a deglaciation. This is illustrated in a hindcast of the LVC deglaciation simulation where all a_{Tatm}^i
 178 are set to 0 K K⁻¹ (Fig. S8).

179 Reconstructions of sea-surface and air temperatures are generally not equally spaced in time. Hence, the
 180 time series are splined using a cutoff period of τ_{cut} years²⁹. τ_{cut} must be chosen appropriately depending on
 181 the resolution of the selected atmosphere and SST time series. A smaller τ_{cut} will result in a better resolved
 182 Ψ'_{AMOC} reconstruction.

183 The sensitivity of SSTs to changes in Ψ'_{AMOC} depends on the location. Some locations are not, or only
 184 weakly sensitive to changes in Ψ'_{AMOC} . At these locations, a_{AMOC} is close to zero. This may lead to large
 185 uncertainties in the AMOC reconstruction, because in this case Eq. (2) approaches singularity. However, as
 186 long as the suite of T'_{oc}^i time series includes data at locations that are sensitive to circulation changes, the
 187 least squares solution of the system of equations will assign very small weights to the time series that are
 188 only weakly sensitive to AMOC.

189 *Data*

190 SST and air temperature data used in the reconstruction (Table S1) were obtained at [http://www.pangaea.](http://www.pangaea.de)
 191 [de, http://www.ncdc.noaa.gov/paleo](http://www.ncdc.noaa.gov/paleo), or by personal communication. See Table S2 for specific links.

Additional information

Supplementary data and information are available in the online version of the paper. Correspondence and requests for materials should be addressed to S.P.R.

Acknowledgements

This study was funded by GRACCIE (CONSOLIDER-INGENIO 2010) and by the Swiss National Science Foundation. We thank F. Joos and C. Waelbroeck for fruitful discussions, M. Steinacher for providing the CSM data, and J. Jouzel for his help with the uncertainties of the ice core data.

Author contributions

S.P.R. and T.F.S. developed the method, A.T. contributed with ideas on method verification and AMOC fingerprinting, S.P.R. performed the B3D simulations, L.M. provided the LVC simulation, J.O.G. provided support of the sediment core data, and S.P.R. and T.F.S. wrote the manuscript. All authors discussed the results and provided input on the manuscript.

Competing financial interests

The authors declare no competing financial interests.

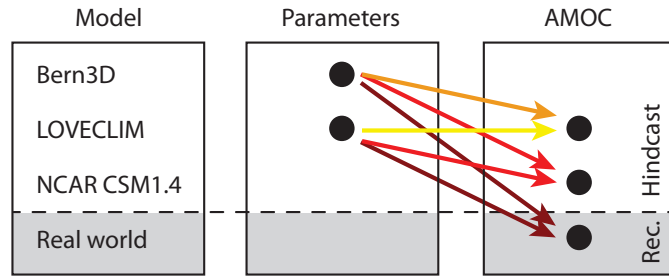


FIG. 1. Overview of the performed AMOC hindcasts and reconstructions. The color of the arrows indicates the order of appearance within the paper (going from light to dark shading). The center column indicates which models are used to calculate the coefficients of the reconstruction scheme. For example, coefficients determined from the Bern3D model are used to hindcast AMOC in LOVECLIM and NCAR models for verification with the directly simulated AMOC in these models, and to reconstruct AMOC from paleoclimate records.

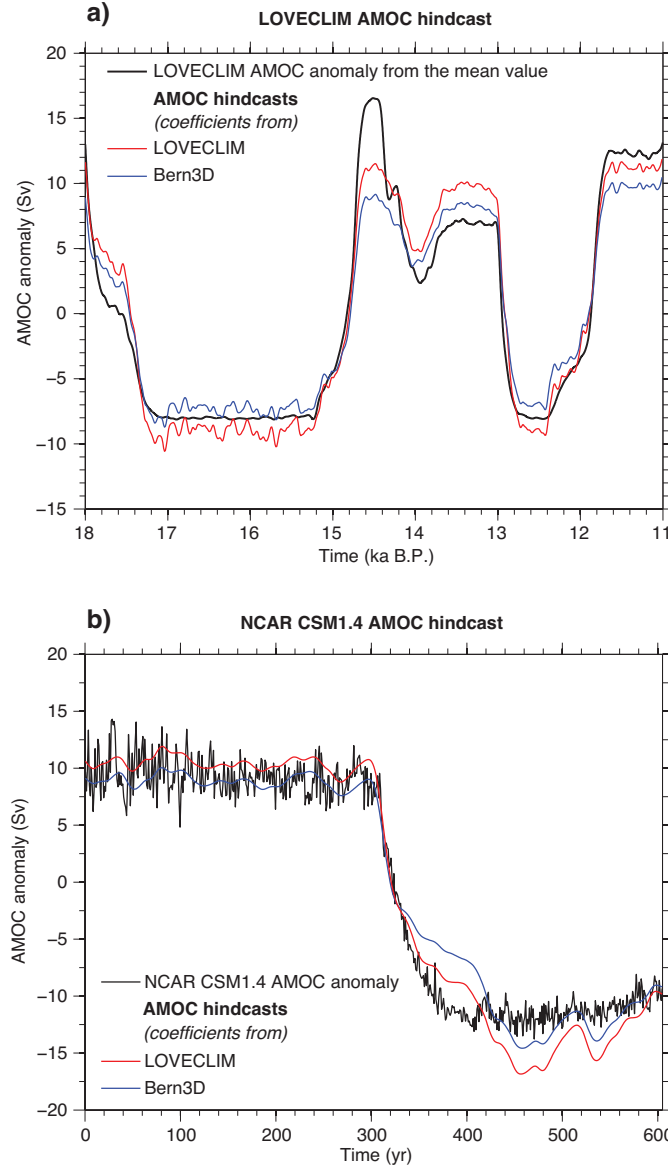


FIG. 2. AMOC hindcasts of two model simulations. The hindcast is given as anomaly from the time series mean value. a) Hindcast of the AMOC of a LOVECLIM deglaciation simulation²³ (Fig. S4) using 14 Atlantic SST time series (Fig. S1). Black line: LOVECLIM AMOC anomaly. Red line: AMOC hindcast calculated from coefficients determined by the LOVECLIM simulation. Blue line: Hindcast from coefficients determined by Bern3D. The coefficients are given in Tables S3 and S4. b) Hindcast of the AMOC of a freshwater forcing simulation²⁴ (Fig. S5). Black line: NCAR CSM1.4 AMOC anomaly. Red line: AMOC hindcast calculated from coefficients determined by LOVECLIM. Blue line: Hindcast from coefficients determined by Bern3D.

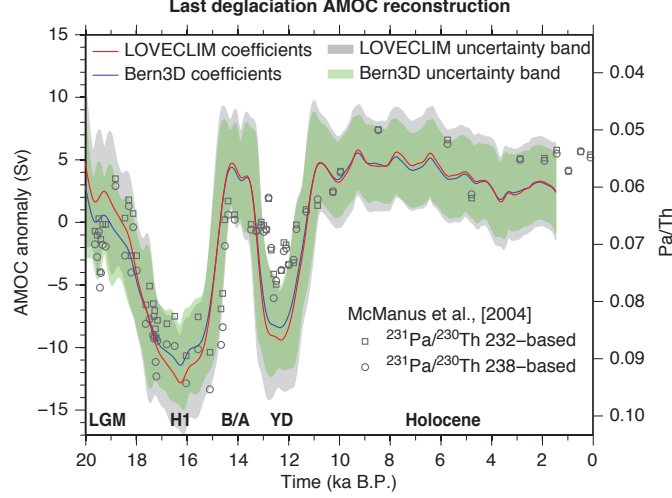


FIG. 3. Reconstruction of the AMOC of the last deglaciation. The reconstruction is given as anomalies from the time series mean value. For the reconstruction, 13 Atlantic SST time series are used (Fig. S1; Table S1) and global mean air temperature, which is determined from the Antarctic air temperature reconstruction from the EPICA Dome C Antarctic ice core²⁵ by applying a polar amplification factor and lowpass filtering the data to remove local-to-hemispheric scale variability. Blue line and green uncertainty band: Reconstruction where the coefficients calculated from Bern3D are used. Red line and gray uncertainty band: Reconstruction where the coefficients calculated from the LOVECLIM model are used. The uncertainty bands are determined by uncertainty propagation of the age-scale uncertainties of ± 500 years, and the uncertainties that arise from the ocean and air temperature time series reconstructions. The uncertainty band of the reconstruction based on Bern3D coefficients additionally includes coefficient uncertainties. The reconstruction shows different AMOC regimes during the Last Glacial Maximum (LGM), Heinrich stadial 1 (H1), the Bølling/Allerød (B/A), the Younger Dryas (YD) stadial, and during the Holocene. Dark gray symbols: Qualitative AMOC reconstruction from sedimentary $^{231}\text{Pa}/^{230}\text{Th}$ ².

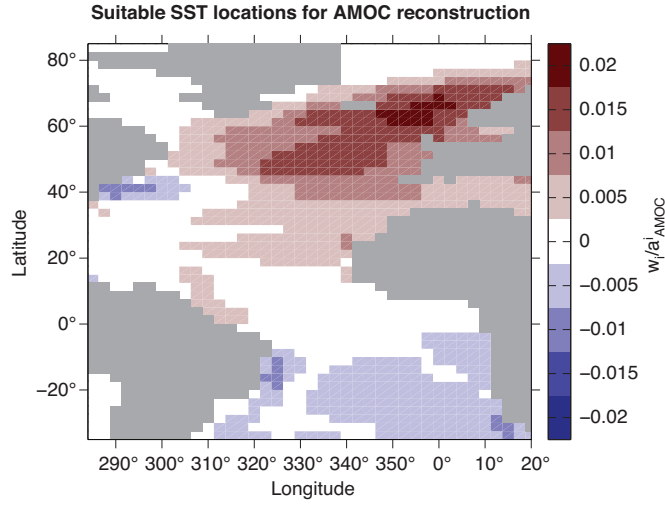


FIG. 4. Suitable locations of SST records for the AMOC reconstruction. An AMOC hindcast of the NCAR CSM1.4 simulation is calculated based on SST time series of every LOVECLIM surface Atlantic model cell and by using reconstruction scheme coefficients determined from the LOVECLIM model. w_i/a_{AMOC}^i is the spatial fingerprint of the AMOC (Eq. 3). It determines the influence of every location i on the AMOC hindcast. The larger the absolute values (the darker the colors), the larger the influence of the location on the AMOC hindcast.

REFERENCES

- 208 1. Lynch-Stieglitz, J. *et al.* Atlantic meridional overturning circulation during the Last Glacial Maximum.
209 *Science* **316**, 66–69 (2007).
- 210 2. McManus, J. F., Francois, R., Gherardi, J.-M. & Keigwin, L. D. Collapse and rapid resumption of
211 Atlantic meridional circulation linked to deglacial climate changes. *Nature* **428**, 834–837 (2004).
- 212 3. Gherardi, J. M. *et al.* Glacial-interglacial circulation changes inferred from Pa-231/Th-230 sedimentary
213 record in the North Atlantic region. *Paleoceanography* **24**, PA2204 (2009).
- 214 4. Lippold, J. *et al.* Strength and geometry of the glacial Atlantic Meridional Overturning Circulation.
215 *Nature Geoscience* **5**, 813–816 (2012).
- 216 5. Robinson, L. F. *et al.* Radiocarbon variability in the western North Atlantic during the last deglaciation.
217 *Science* **310**, 1469–1473 (2005).
- 218 6. Scholten, J. C. *et al.* Advection and scavenging: Effects on ^{230}Th and ^{231}Pa distribution off Southwest
219 Africa. *Earth and Planetary Science Letters* **271**, 159 – 169 (2008).
- 220 7. Keigwin, L. D. & Boyle, E. A. Did North Atlantic overturning halt 17,000 years ago? *Paleoceanography*
221 **23**, PA1101 (2008).
- 222 8. Lippold, J. *et al.* Does sedimentary $^{231}\text{Pa}/^{230}\text{Th}$ from the Bermuda rise monitor past atlantic meridional
223 overturning circulation? *Geophysical Research Letters* **36**, L12601 (2009).
- 224 9. Ganachaud, A. & Wunsch, C. Improved estimates of global ocean circulation, heat transport and mixing
225 from hydrographic data. *Nature* **408**, 453–456 (2000).
- 226 10. Trenberth, K. & Caron, J. M. Estimates of meridional atmosphere and ocean heat transports. *Journal*
227 *of Climate* **14**, 3433–3443 (2001).
- 228 11. NGRIP members. High-resolution record of Northern Hemisphere climate extending into the last inter-
229 glacial period. *Nature* **431**, 147–151 (2004).

- 230 12. Schulz, H., von Rad, U. & Erlenkeuser, H. Correlation between Arabian Sea and Greenland climate
231 oscillations of the past 110,000 years. *Nature* **393**, 54–57 (1998).
- 232 13. Peterson, L. C., Haug, G. H., Hughen, K. A. & Röhl, U. Rapid changes in the hydrologic cycle of the
233 tropical Atlantic during the last glacial. *Science* **290**, 1947–1951 (2000).
- 234 14. Wang, Y. J. *et al.* A high-resolution absolute-dated Late Pleistocene monsoon record from Hulu Cave,
235 China. *Science* **294**, 2345–2348 (2001).
- 236 15. EPICA Community Members. One-to-one coupling of glacial climate variability in Greenland and
237 Antarctica. *Nature* **444**, 195–198 (2006).
- 238 16. Stocker, T. F. & Johnson, S. J. A minimum thermodynamic model for the bipolar seesaw. *Paleoceanog-*
239 *raphy* **18**, 1087 (2003).
- 240 17. Stocker, T. F. Past and future reorganizations in the climate system. *Quaternary Science Reviews* **19**,
241 301–319 (2000).
- 242 18. Hemming, S. R. Heinrich events: Massive late Pleistocene detritus layers of the North Atlantic and their
243 global climate imprint. *Reviews of Geophysics* **42**, RG1005 (2004).
- 244 19. Broecker, W. S. Was the Younger Dryas triggered by a flood? *Science* **312**, 1146–1148 (2006).
- 245 20. Barber, D. C. *et al.* Forcing of the cold event of 8,200 years ago by catastrophic drainage of Laurentide
246 lakes. *Nature* **400**, 344–348 (1999).
- 247 21. Ritz, S. P., Stocker, T. F. & Joos, F. A coupled dynamical ocean – energy balance atmosphere model
248 for paleoclimate studies. *Journal of Climate* **24**, 349–375 (2011).
- 249 22. Masson-Delmotte, V. *et al.* EPICA Dome C record of glacial and interglacial intensities. *Quaternary*
250 *Science Reviews* **29**, 113–128 (2010).
- 251 23. Menviel, L., Timmermann, A., Elison Timm, O. & Mouchet, A. Deconstructing the Last Glacial ter-
252 mination: the role of millennial and orbital-scale forcings. *Quaternary Science Reviews* **30**, 1155–1172
253 (2011).

- 254 24. Bozbiyik, A., Steinacher, M., Joos, F., Stocker, T. F. & Menviel, L. Fingerprints of changes in the
255 terrestrial carbon cycle in response to large reorganizations in ocean circulation. *Climate of the Past* **7**,
256 319–338 (2011).
- 257 25. Jouzel, J. *et al.* Orbital and millennial Antarctic climate variability over the past 800,000 years. *Science*
258 **317**, 793–796 (2007).
- 259 26. Rayner, D. *et al.* Monitoring the Atlantic meridional overturning circulation. *Deep Sea Research Part*
260 *II: Topical Studies in Oceanography* **58**, 1744–1753 (2011).
- 261 27. Okazaki, Y. *et al.* Deepwater formation in the North Pacific during the last glacial termination. *Science*
262 **329**, 200–204 (2010).
- 263 28. Shakun, J. D. & Carlson, A. E. A global perspective on Last Glacial Maximum to Holocene climate
264 change. *Quaternary Science Reviews* **29**, 1801–1816 (2010).
- 265 29. Enting, I. G. On the use of smoothing splines to filter CO₂ data. *Journal of Geophysical Research* **92**,
266 10,977–10,984 (1987).